Spinodal decomposition in multicomponent polymer blends

C. C. Lin, H. S. Jeon, and N. P. Balsara[a)]
Department of Chemical Engineering, Polytechnic University, Six Metrotech Center, Brooklyn, New York 11201

B. Hammouda
National Institute of Standards and Technology, Building 235, E 151, Gaithersburg, Maryland 20899

(Received 9 February 1995; accepted 18 April 1995)

Spinodal decomposition in multicomponent mixtures of two homopolymers and a block copolymer was studied by a combination of neutron and light scattering experiments. Mixtures of nearly monodisperse polyolefins—polymethylbutylene ($M_w=1.7\times10^5$ gm/mol), polyethylbutylene ($M_w=2.2\times10^5$ gm/mol), and a symmetric polymethylbutylene-*block*-polyethylbutylene ($M_w=4.6\times10^4$ gm/mol) were studied, following relatively deep quenches into the spinodal region $-\chi/\chi_s$ ranged from 1.7 to 2.4 (χ is the Flory–Huggins interaction parameter at the experimental temperature and χ_s is the Flory–Huggins interaction parameter at the spinodal temperature). The ratio of homopolymer volume fractions was kept constant at unity, and the block copolymer volume fraction was varied from 0.0 to 0.2. The evolution of structure was followed over five decades of real time—1 min to 1 month. During this time, the characteristic length scale of the phase separated structure increased from 10^{-1} to 10 μm. The early stages of spinodal decomposition, captured by time-resolved neutron scattering, were compared with theoretical predictions based on the random phase approximation (RPA). Qualitative agreement was obtained. The intermediate and late stages, studied by light scattering, followed classic signatures of binary spinodal decomposition. Experimental evidence indicates that the block copolymer is uniformly distributed throughout the sample during all stages of the decomposition. © *1995 American Institute of Physics.*

INTRODUCTION

The relationship between thermodynamics and morphology of polymer blends is of practical and fundamental importance.[1,2] Designing processes to achieve a particular morphology requires an understanding of phase separation kinetics and thermodynamic interactions in polymer mixtures. Theoretical descriptions of polymer mixtures based on the random phase approximation (RPA) have been crucial in this respect.[3] This approach has provided a remarkably accurate description of the concentration fluctuations in single-phase polymer mixtures. In addition, RPA provides the starting point for quantifying the evolution of structure when polymer mixtures are quenched from the single-phase to the two-phase region of the phase diagram.[4–6]

Most of experimental work on polymer blends, both in the single-phase region[7–19] as well as in the two-phase region,[20–27] is restricted to binary blends. In a previous publication,[28] we examined the concentration fluctuations in multicomponent blends of two homopolymers and a block copolymer. Homogeneous mixtures of nearly monodisperse, model polyolefins—polymethylbutylene (PM), polyethylbutylene (PE), and polymethylbutylene-*block*-polyethylbutylene (PM-PE)—were studied as a function of PM-PE concentration. Multicomponent concentration fluctuations are characterized by a matrix of partial structure factors.[29–32] Individual elements of this matrix were obtained from SANS measurements, using contrast matching techniques. We found that these mixtures contained large amplitude fluctuations in homopolymer concentrations—$\phi_{\rm PM}$ and $\phi_{\rm PE}$ (ϕ_i is the volume fraction of component i, i=PM, PE, or PM-PE). In contrast, the concentration fluctuations in $\phi_{\rm PM\text{-}PE}$ were negligibly small. This situation is depicted schematically in Fig. 1(a). We assume incompressibility ($\phi_{\rm PE}+\phi_{\rm PM}+\phi_{\rm PM\text{-}PE}=1$, everywhere), so the system is completely described by two concentration variables: $\phi_{\rm PM}$ and $\phi_{\rm PM\text{-}PE}$.

In this paper we study the evolution of structure of PM/PE/PM-PE mixtures after they have been quenched from the homogeneous state into the spinodal region (spinodal decomposition). The molecular weights of the PM and PE homopolymers are larger than those used in our previous study (Ref. 28), corresponding to a χN of about 4 at room temperature (χ is the Flory–Huggins interaction parameter and N is the number of monomers per chain in the homopolymers). The early stages of the spinodal decomposition occur via amplification of Fourier components of composition fluctuations that were present prior to the quench.[33,34] Morral and Cahn have studied some of the theoretical aspects of spinodal decomposition in incompressible ternary mixtures.[35] In principle, the concentration fluctuations of both PM and PM-PE could grow in the spinodal region. Two extreme possibilities for the distribution of components are shown in Fig. 1. One possibility is that the block copolymer is uniformly distributed [Fig. 1(b)]. In this case, the system can be described in terms of a single concentration variable—$\phi_{\rm PM}$—because $\nabla\phi_{\rm PM\text{-}PE}\approx0$. This is analogous to spinodal decomposition in incompressible, binary blends, and we refer to this as a pseudobinary situation. The other possibility is the block copolymer is located at the interface between the PM-rich and PE-rich phases [Fig. 1(c)]. In this case, both $\nabla\phi_{\rm PM}$ and $\nabla\phi_{\rm PM\text{-}PE}$ are nonzero. For the situation

a)Author to whom correspondence should be addressed.

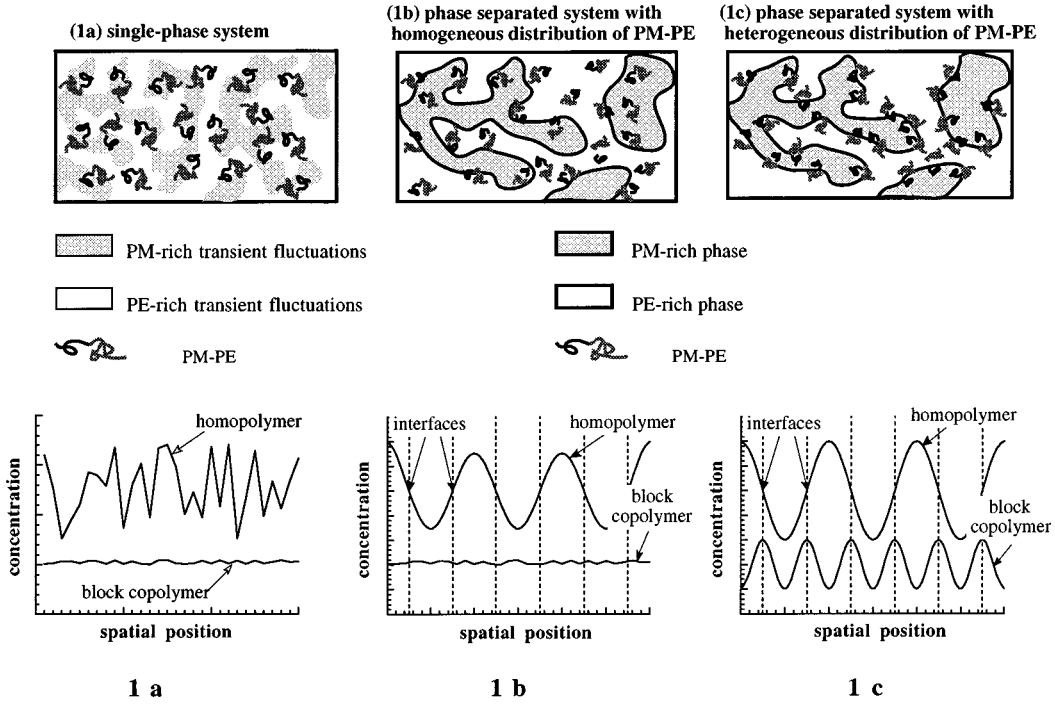

FIG. 1. Schematic representation of concentration fluctuations in multicomponent mixtures of two homopolymers and a block copolymer: PM/PE/PM-PE. (a) Single-phase systems with large homopolymer concentration fluctuations, but the block copolymer is homogeneously distributed. This figure is based on data given in Ref. 28. (b) Phase separated mixtures in which the block copolymer is uniformly distributed in both phases. (c) Phase separated mixtures in which the block copolymer is preferentially located at the interface.

depicted in Fig. 1(c), the characteristic length scale of the periodic PM-PE concentration profile is half that of the PM profile. There is an infinitum of intermediate possibilities in which only partial segregation of the block copolymer takes place.

The characteristics of the spinodal decomposition in PM/PE/PM-PE mixtures were studied by a combination of neutron and light scattering experiments. We report on the evolution of the characteristic length scale of the decomposed structure as well as the location of the block copolymer within this structure. Time scales covered in this study range from 1 to 10^5 min (i.e., 1 min to 1 month). The characteristic length scale of the phase separated structure increased from 10^{-1} to 10 μm during this time.

Experiments demonstrating that spinodal decomposition in polymer mixtures is fundamentally similar to that in low molecular weight mixtures were performed many years ago by Nishi *et al.*[20] Since then several researchers have studied this phenomenon. Hashimoto and co-workers[21] and Han and co-workers[22] have conducted a systematic study of the spinodal decomposition in polystyrene/polyvinylmethylether blends using light scattering. Bates and Wiltzius have studied phase separation in mixtures of protonated and deuterated polybutadiene.[23] Recently, time-resolved neutron scattering has been used to study the early stages of spinodal decomposition.[24–27] Spinodal decomposition in mixtures of two homopolymers and a block copolymer were first studied by Roe and co-workers.[36,37] These experiments demonstrated that the addition of a high molecular weight block copolymer (M_n of block copolymer was a factor of 5 larger than that of the homopolymers) retards the kinetics of phase separation. Similar results were obtained by Hashimoto and Izumitani.[38,39]

EXPERIMENTAL SECTION

Materials and sample preparation

Nearly monodisperse model polyolefins were synthesized following the methodology of Rachapudy *et al.*[40] Homopolymers—polymethylbutylene and polyethylbutylene—were synthesized in two steps using isoprene and ethylbutadiene, respectively, as monomers. The polymerizations were conducted under high vacuum[41] in cyclohexane and the polydienes consisted of predominantly (93%) 1,4 addition. Separate aliquots of the polydienes were then saturated in the presence of a palladium catalyst with H_2 and D_2 to yield fully hydrogenated and partially deuterated polyolefins.

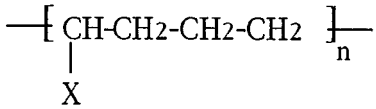

model polyolefin

X=CH_3 - poly(methyl butylene) (PM)

X=C_2H_5 - poly(ethyl butylene) (PE)

A pair of diblock copolymers—*h*PM-*h*PE and *d*PM-*d*PE—were synthesized by sequential anionic polymerization of isoprene and ethylbutadiene, followed by saturation. These polyolefins are essentially derivatives of polyethylene and are chemically equivalent to alternating ethylene–

TABLE I. Characterization of polymers.

Sample designation	Density[a] (gm/cm^3)	n_D[b]	Molecular weight[c]	Polydispersity index[d]	Polymerization index (N_i, N_{ib})	Vol. fr. of PM in block copolymer[f]
*h*PM-*A*	0.8540	⋯	7.7×10^4	1.06	1105	⋯
*d*PM-*A*	0.9226	5.52	8.4×10^4	1.06	1105	⋯
*h*PM-*B*	0.8540	⋯	1.73×10^5	1.07	2500	⋯
*d*PM-*B*	0.9300	6.11	1.88×10^5	1.07	2500	⋯
*h*PE-*A*	0.8629	⋯	4.8×10^4	1.07	575	⋯
*d*PE-*A*	0.9297	6.38	5.2×10^4	1.07	575	⋯
*h*PE-*B*	0.8628	⋯	2.21×10^5	1.08	2600	⋯
*d*PE-*B*	0.9272	6.15	2.38×10^5	1.08	2600	⋯
*h*PM-*h*PE	0.8579	⋯	4.6×10^4	1.09	300–300[e]	0.452
*d*PM-*d*PE	0.9007	3.67	4.8×10^4	1.09	300–300[e]	0.452

[a]Using a density gradient column.
[b]Average number of deuterium per monomer, based on density measurements.
[c]From light scattering on polydiene precursors.
[d]From GPC, based on polyisoprene calibration, uncorrected for column dispersion.
[e]Polymerization index of both blocks was 300.
[f]Based on ^{13}C NMR on *h*PM-*h*PE, and densities of *h*PM and *h*PE.

propylene and ethylene–butene copolymers. In this paper we refer to the poly(methyl butylene) chains as PM and the poly(ethyl butylene) chains as PE, where the letters *M* and *E* refer to the methyl and ethyl branches emanating from the C–C backbone.

The characteristics of the polymers were determined using procedures described in Ref. 28 and are listed in Table I. Polymers are named on the basis of their composition. The prefix *h* refers to hydrogenated polymers and the prefix *d* refers to partially deuterated polymers. Note that there is no neutron contrast between the blocks in both *h*PM-*h*PE and *d*PM-*d*PE (see Ref. 28 for characterization details of this polymer). Two pairs of PM and PE homopolymers were synthesized. The letter *A* identifies the lower molecular weight species, while the letter *B* identifies the higher molecular weight species. Homogeneous PM-*A*/PE-*A*/PM-PE mixtures were used to obtain χ parameters. The spinodal decomposition studies were performed on PM-*B*/PE-*B*/PM-PE mixtures.

Blends were made by dissolving the components in cyclohexane and then drying to constant weight in a vacuum oven at 70 °C. Small-angle neutron scattering (SANS) and small-angle light scattering (SALS) experiments were conducted on 1 mm thick samples held between quartz windows separated by an aluminum spacer. Samples for the wide-angle light scattering (WALS) experiments were confined to heat sealed glass cuvettes with a 0.74 mm inner diameter. The composition of the blends examined in this paper are listed in Table II.

Spinodal decomposition studies were performed on blends that were annealed at a temperature well above its phase-transition temperature for 15 h and then quenched to room temperature as quickly as possible. The annealing temperatures ranged from 170 to 250 °C. GPC measurements confirmed that our thermal treatment did not cause polymer degradation. All the spinodal decomposition experiments were conducted at room temperature which varied between 22 and 25 °C.

Time resolved scattering from blends undergoing spinodal decomposition

The 30 m small angle neutron scattering (SANS) machine on the NG3 beamline at the National Institute of Standards and Technology[42] was used to study the early stage of spinodal decomposition. The following instrument configuration was used: neutron wavelength, $\lambda=10$ or 12.5 Å, wavelength spread, $\Delta\lambda/\lambda=0.15$, sample-to-detector distance $=13.17$ m, sample aperture$=0.635$ cm, source-to-sample distance$=11$ m, and source size$=5$ cm. The instrument configuration used in these measurements allowed access to q values as low as 20 μm^{-1}. The scattering data were corrected for background, empty cell scattering and detector sensitiv-

TABLE II. Summary of blends examined in this paper.

Experiments	Blend designation	Components			ϕ_A/ϕ_B[a]	ϕ_{AB}[a]
		A	*B*	*A*–*B*		
Spinodal decomposition	A0	*d*PM-*B*	*h*PE-*B*		1.0	0.0
	A10	*d*PM-*B*	*h*PE-*B*	*h*PM-*h*PE	1.0	0.1
	A20	*d*PM-*B*	*h*PE-*B*	*h*PM-*h*PE	1.0	0.2
	B10	*h*PM-*B*	*h*PE-*B*	*d*PM-*d*PE	1.0	0.1
Determination of χ parameters	C20	*d*PM-*A*	*h*PE-*A*	*h*PM-*h*PE	1.3	0.2
	D20	*h*PM-*A*	*h*PE-*A*	*d*PM-*d*PE	1.3	0.2

[a]Based on weight fractions, assuming no volume change on mixing.

ity. Since we were mainly interested in *relative* changes in the scattering profiles (peak position and intensity), the data were not scaled to absolute cross section.

The wide angle light scattering (WALS) measurements were made on an ALV-5000 instrument at the Polytechnic University. The sample, encased in a cylindrical cuvette, was immersed in an index matching, thermostated bath. The sample was located at the center of a computer driven goniometer equipped with 400 μm pinholes, a focusing lens to image the scattered light on to the face of a photomultiplier supplied by EMI. The samples were probed using light with $\lambda=0.63$ μm from a HeNe laser.

The small angle light scattering (SALS) apparatus was designed to obtain the scattering profiles from flat samples. Samples used in these experiments were identical to those used in the SANS experiments. This apparatus was used to follow the late stages of spinodal decomposition. At this stage, the scattered intensity was quite large, and scattering profiles were obtained by translating a photodiode vertically. The data were recorded on a Macintosh IIci using Labview. Background scattering was negligible in the light scattering experiments, and the measured data were only corrected for changes in sample transmission. In both WALS and SALS, the intensity of the incident beam was monitored with the help of a beam spliter and a reference diode.

All the scattering experiments reported in this paper were repeated several times. For the sake of clarity, data obtained from only one of the runs is shown. In this paper we focus on the location of the scattering maximum and the peak intensity, which were reproducible to within 10%.

Static small angle neutron scattering

The 8 m SANS machine on the NG5 beamline at the National Institute of Standards and Technology was used to obtain the absolute SANS intensity from the multicomponent blends. These experiments were used to study the concentration fluctuations of individual components in both single-phase as well as two-phase systems, and to determine χ parameters. The following instrument configuration was used: neutron wavelength, $\lambda=9.0$ Å wavelength spread, $\Delta\lambda/\lambda=0.25$, sample-to-detector distance=3.6 m, sample aperture =1.2 cm, source-to-sample distance=4.1 m, and source size =2.7 cm. The scattering data were corrected for background, empty cell scattering and detector sensitivity, converted to an absolute scale using secondary standards, and azimuthally averaged. The incoherent scattering for each blend was estimated from SANS measurements on pure hPM, assuming that it is proportional to the concentration of H atoms in the blend, and subtracted from the azimuthally averaged scattering profiles to give the coherent scattering intensity, $I(q)$ [$q=4\pi\sin(\theta/2)/\lambda$, where θ is the scattering angle]. The absolute scattered intensity was thus obtained without resorting to any adjustable parameters.

PHASE DIAGRAM OF PM/PE/PM-PE MIXTURES

In this section we map out the phase diagram of PM-*B*/PE-*B*/PM-PE mixtures. This is necessary for interpretation of the spinodal decomposition experiments. Pioneering experiments by Cohen and Ramos demonstrated the richness of phase diagrams of mixtures of two homopolymers and a block copolymer.[43,44] Theoretical analyses by Leibler[45] and Broseta and Fredrickson,[46] which apply to homogeneous phases, predict that both biphasic and triphasic equilibria are possible in these systems. On the other hand, if the coexisting phases are not homogeneous and the block copolymer is located at the intervening interface, then it is possible to obtain emulsified phases of one polymer in another.[47,48]

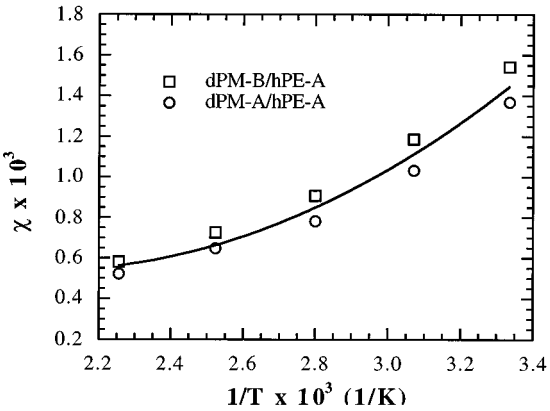

FIG. 2. The dependence of χ parameter on temperature (T) obtained from binary mixtures of dPM-A/hPE-A and dPM-B/hPE-A. It is apparent that the χ parameter is nearly independent of component molecular weight.

The starting point of these analyses is the Flory–Huggins theory which describes the free energy of a mixing of two homopolymers (A and B) and a diblock copolymer (AB), ΔG_m[49–52]

$$g(\phi_A,\phi_{AB})=\frac{\Delta G_m}{\upsilon kT}=\frac{\phi_A\ln\phi_A}{N_A\upsilon_A/\upsilon}+\frac{\phi_{AB}\ln\phi_{AB}}{N_{Ab}\upsilon_A/\upsilon+N_{Bb}\upsilon_B/\upsilon}+\frac{(1-\phi_A-\phi_{AB})\ln(1-\phi_A-\phi_{AB})}{N_B\upsilon_B/\upsilon}+\chi[\{\phi_A+f\phi_{AB}\}\{1-\phi_A-\phi_{AB}+(1-f)\phi_{AB}\}-f(1-f)\phi_{AB}], \quad (1)$$

where $g(\phi_A,\phi_{AB})$ is the normalized free energy of mixing per unit volume, k is the Boltzmann constant, T is the absolute temperature, N_i and ϕ_i are the number of monomers per chain and volume fraction of component i, respectively, ($i=A,B$), ϕ_{AB} is the volume fraction of the block copolymer, N_{Ab} and N_{Bb} are the number of A and B monomers in a block copolymer chain, respectively, f is the volume fraction of A mers in the block copolymer, υ_A and υ_B are the volumes occupied by monomers A and B, respectively, and χ is the Flory–Huggins interaction parameter between A and B monomers based on a reference volume, υ. The reference volume throughout this paper is equal to 148.6 Å^3, which is equal to the geometric mean of the volumes of C_5 and C_6 units in PM and PE chains at 27 °C, respectively.

In Fig. 2 we summarize static SANS data obtained from binary blends of d PM-A/h PE-A and d PM-B/h PE-A ($\phi_{PM}/\phi_{PE}=1.0$). The SANS data from the binary mixtures were recast in terms of the Flory–Huggins interaction parameter, χ, using procedures given in Ref. 28. It is evident

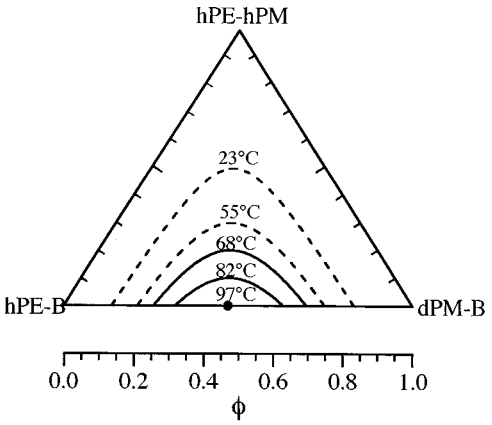

FIG. 3. The predicted spinodal curves of the ternary blend *d*PM-*B*/*h*PE-*B*/*h*PM-*h*PE at temperatures ranging from 25 to 170 °C. The spinodal decomposition experiments reported here are carried out on blends containing 0%, 10%, and 20% by volume of block copolymer ($\phi_{PM}/\phi_{PE}=1.0$) at 25 °C. The solid lines represent predicted spinodal curves at temperatures corresponding to the critical points of these mixtures. The point at the base of the ternary phase diagram indicates the spinodal temperature of the binary blend of *d*PM-*B*/*h*PE-*B*.

that χ is, within experimental error, independent of molecular weight of the *d* PM chains. The temperature dependence of χ can be approximated as follows:

$$\chi=2.82\times10^{-3}-2.231/T+545.5/T^2. \tag{2}$$

Equation (2) represents the best quadratic fit through the data in Fig. 2.

The spinodal line for PM/PE/PM-PE mixtures is given by

$$\left(\frac{\partial^2 g}{\partial\phi_A^2}\right)\left(\frac{\partial^2 g}{\partial\phi_{AB}^2}\right)-\left(\frac{\partial^2 g}{\partial\phi_A\partial\phi_{AB}}\right)^2=0. \tag{3}$$

Predictions of the spinodal curves for PM-*B*/PE-*B*/PM-PE mixtures at several temperatures were calculated using Eqs. (1)–(3). The results are shown on a ternary phase diagram in Fig. 3. For the molecular weight and temperature range of interest, the Flory–Huggins predictions for the phase diagrams are relatively simple. For phase separated systems, two-phase equilibrium is predicted over the accessible composition and temperature window. The tie lines are nearly horizontal owing to the fact that the molecular volumes of PM-*B* and PE-*B* are nearly identical and because the block copolymer is nearly symmetric (see Table I). The calculated spinodal temperatures, T_s, for blends with $\phi_{PM\text{-}B}/\phi_{PE\text{-}B}=1.0$ and $\phi_{PM\text{-}PE}=0.0$, 0.1, and 0.2 blends are given in Table III.

TABLE III. Summary of static SANS results.

	T_s(°C)		χ/χ_s	
Blend	Calculated	Measured	Calculated	Measured
A0	97±10	130±10	1.94	2.35
A10	82±9	95±9	1.75	1.92
A20	68±9	80±10	1.55	1.72

The spinodal temperatures for these blends were also determined experimentally. SANS profiles were compared with theoretical predictions based on RPA and departures between experiment and theory were used as a signature of the onset of phase separation. The RPA prediction for the scattered intensity for a single-phase, multicomponent mixture is given by[29–32]

$$I(q)=B^T S(q) B, \tag{4}$$

where the multicomponent structure factor matrix, $S(q)$, is given by

$$S(q)=[S^0(q)^{-1}+V(q)]^{-1}. \tag{5}$$

Matrix S^0 is related to ideal intramolecular correlations in the absence of interactions ($\chi=0$), V is related to the interaction parameters between the constituent monomers, and the vector B characterizes the scattering contrasts in the system. For an incompressible mixture of two homopolymers and a diblock copolymer, S^0 and V are 3×3 matrices and B is a 3 component vector. Expressions for the elements of S^0, V, and B, and parameters required to specify the components of these matrices for the PM-*B*/PE-*B*/PM-PE system are given in Ref. 28. Parameters used in these calculations are given in Appendix A.

SANS profiles of A0, A10, and A20 samples were measured as a function of increasing temperature. Samples were annealed at each temperature for at least 100 min before the SANS data were acquired. In Fig. 4(a) we plot $I(q)$ vs q obtained from the blend A20 at selected temperatures. The scattering profiles at all temperatures are qualitatively similar and show a monotonic decrease with increasing q. It is evident that $I(q)$ obtained at the higher temperatures (70 °C and above) are nearly superposable. The scattering profile obtained at 50 °C, however, shows significant deviations.

The distinction between the scattering profiles becomes clearer when we plot the data in the Kratky format: Iq^2 vs q. In the single phase region, the product Iq^2 is predicted by RPA to reach a plateau at high q (the Kratky plateau). Only the statistical segment lengths and monomer volumes affect the value of the Kratky plateau.[3] Since these are weak functions of temperature, the product Iq^2 is also expected to be a weak function of temperature in the single-phase region. The SANS data from the A20 blend is compared with theoretical predictions in Fig. 4(b). It is evident that $I(q)q^2$ approaches a plateau of about 130 μm^{-3} at 90 °C and above, a value that is in good agreement with RPA predictions [see Fig. 4(b)]. However, it drifts to lower values at temperatures less than or equal to 70 °C. The SANS data obtained from A0 and A10 blends showed similar trends.

The temperature dependence of the Kratky plateau of all three blends is summarized in Fig. 5. The value of the plateau reported, P, is the average of $I(q)q^2$ in the range $160<q<400$ μm^{-1}. The ordinate in Fig. 5 is normalized by a constant P_h—the average value of P at high temperatures. The transition temperature from single phase to two phase, T_s, is estimated to be the point of departure of normalized P from unity (by 5% or more). Since this departure is not abrupt and our choice of 5% is based on estimated experimental errors, there is considerable uncertainty associated

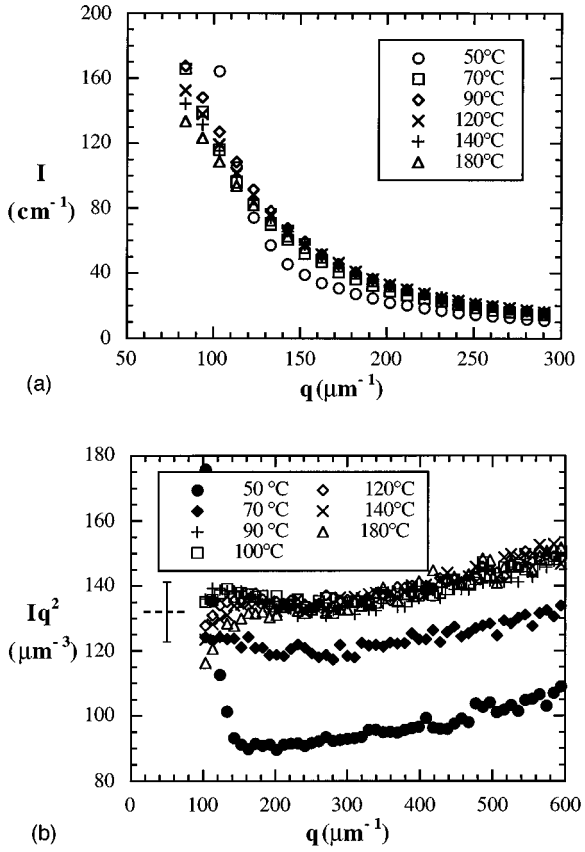

FIG. 4. SANS profiles of blend A20 at selected temperatures. (a) I vs q plot. (b) Iq^2 vs q plot (Kratky format). The dashed line represents the RPA based estimate of the Kratky plateau at 170 °C and the error bar represents the uncertainty in this estimate due, mainly to errors in instrument calibration and characterization. The drift of Iq^2 at large q may be due to small errors in background subtraction.

with our measurements of T_s. Nevertheless, we observed a systematic trend toward lower phase transition temperatures with increasing block copolymer concentration. The experimentally determined values of T_s are listed in Table III. The experimental trends for the dependence of T_s on ϕ_{AB} parallel

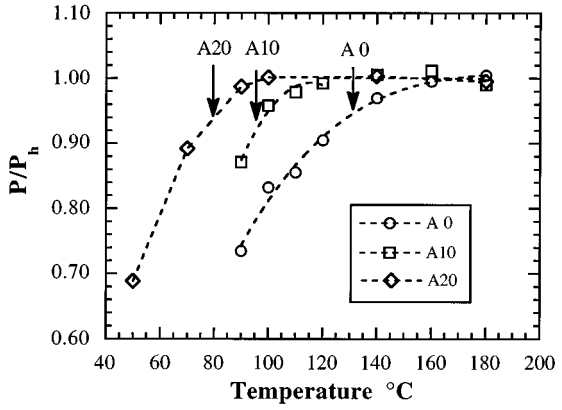

FIG. 5. The temperature dependence of the Kratky plateau (P) for blends A0 (circles), A10 (squares), and A20 (diamonds). The ordinate is normalized by P_h, the average value of P at high temperatures. For A0, P_h=132.6 μm^3. For A10, P_h=137.4 μm^3. For A20, P_h=130.5 μm^3. [Actual plateau=(normalized)$P\times(P_h)$.]

theoretical predictions. The differences between experiment and predictions are within error bounds for two out of the three samples. One of the reasons for obtaining T_s was to estimate the thermodynamic driving force for phase separation at room temperature, gauged by the magnitude of χ/χ_s (where χ_s is the value of χ at the spinodal). The theoretical and experimental values of χ/χ_s, based on Eq. (2), are also listed in Table III.

Light scattering is the experiment of choice for determining the phase transition temperature of a mixture. The absence or presence of a spinodal ring is an unambiguous way of determining whether or not a blend with critical composition is single phase. However, due to the high molecular weights of the components, such determination would require very long experiments, lasting several months per sample.[53] All of the light scattering results presented here were obtained at room temperature, which is well below T_s of all the samples.

EQUATIONS DESCRIBING THE EARLY STAGES OF SPINODAL DECOMPOSITION

Spinodal decomposition occurs via growth of concentration fluctuations that are present in the single-phase region, before the system is quenched into the unstable region of the phase diagram. We thus need to determine concentration fluctuations in ϕ_{PM} and $\phi_{\mathrm{PM\text{-}PE}}$ in homogeneous PM/PE/PM-PE mixtures. The concentration fluctuations in homogeneous PM-*A*/PE-*A*/PM-PE mixtures at room temperature were described in Ref. 28. We briefly review the arguments presented there, and extend our investigation to higher temperatures (up to 170 °C).

In Fig. 6(a) we show SANS intensities from two single-phase PM-*A*/PE-*A*/PM-PE blends, with $\phi_{\mathrm{PM}}/\phi_{\mathrm{PE}}=1.3$ and $\phi_{\mathrm{PM\text{-}PE}}=0.2$ (see Table II). These are blends composed of the lower molecular weight homopolymers at the critical ratio. The only difference between the two blends—labeled C20 and D20—is that in blend C20 the PM homopolymer is labeled with deuterium, while in blend D20, the PM-PE block copolymer is labeled. The SANS data from these two blends allow us to study correlations of individual components in the multicomponent mixture. The measured SANS profiles from the two blends differ substantially, indicating a qualitative difference in the correlations of the homopolymer (PM) and the block copolymer (PM-PE). Correlations in polymer mixtures arise due to connectivity of the chains and due to concentration fluctuations. In order to estimate the amplitude of the concentration fluctuations we must subtract out the connectivity contribution to the SANS signal. The dashed lines are the calculated intensities for blends C20 and D20 using Eqs. (4) and (5) with all the χ parameters are set to zero. This represents the RPA based estimate of the contribution to $I(q)$ due to connectivity, and we refer to this as $I_{\mathrm{ideal}}(q)$. The excess scattering $E(q)$, defined by

$$E(q)=I(q)-I_{\mathrm{ideal}}(q), \tag{6}$$

is thus a measure of the magnitude of the concentration fluctuations. Note that when we use the χ parameters given in Table V, the RPA based estimate of $I(q)$, represented by the solid line in Fig. 6(a), is in very good agreement with the

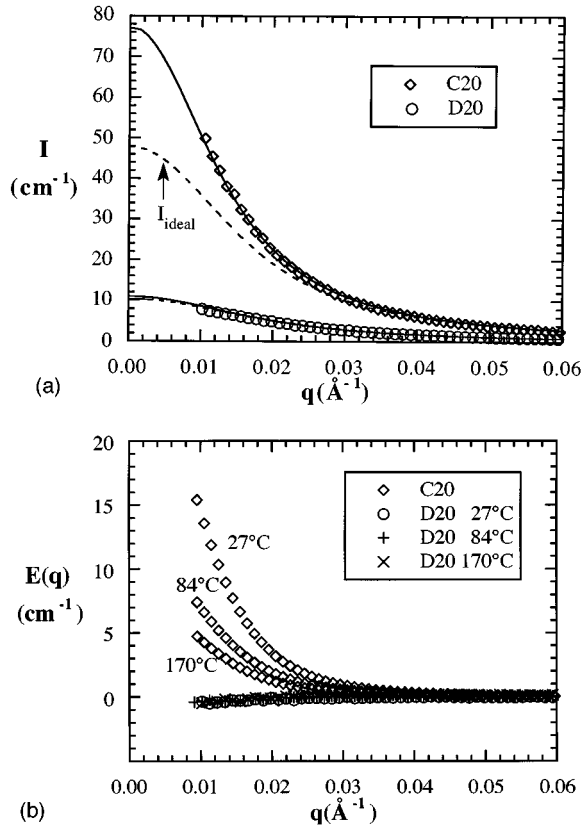

FIG. 6. (a) The SANS data and multicomponent RPA predictions (solid lines) from ternary blends of C20 (diamonds) and D20 (circles) at 27 °C. Both blends contain 20% diblock copolymer, but in blend C20 the deuterium labels are on homopolymer PM-*A*, while in blend D20, the deuterium labels are of the block copolymer PM-PE. The dashed lines represent I_{ideal}, the scattering contribution due to chain connectivity, and were calculated using multicomponent RPA with all χ_s set to zero for both blends. (b) The excess scattering $E(q)$ of blends C20 and D20 at selected temperatures [see Eq. (6) for definition of $E(q)$].

experimental data. This enhances our confidence in our estimate of $I_{\text{ideal}}(q)$. We plot $E(q)$ vs q obtained from blends C20 and D20 at selected temperatures in Fig. 6(b). The value of $E(q)$ of blend D20 is virtually zero at all q and at all temperatures. This indicates that the block copolymer concentration fluctuations are negligibly small. In contrast, we see significant excess scattering in blend C20 at $q<30\ \mu\text{m}^{-1}$ at all temperatures. This indicates that there are substantial homopolymer concentration fluctuations with length scale greater than 0.2 μm ($2\pi/q$). We thus conclude that in single phase, critical PM/PE/PM-PE blends the homopolymer concentration fluctuations are of much larger amplitude than that of block copolymer concentration fluctuations, regardless of temperature.

Given the fact that the block copolymer is uniformly distributed in the single-phase PM/PE/PM-PE blends, and the fact that the predicted equilibrium consists of phases with equal concentrations of block copolymer (see section on phase diagram of PM/PE/PM-PE mixtures), it is reasonable to assume that the early stages of spinodal decomposition is dominated by growth of homopolymer concentration fluctuations, only. This is the pseudobinary condition with only one independent concentration variable, i.e., ϕ_A [Fig. 1(b)]. We can thus use the Cahn analysis of spinodal decomposition in binary mixtures.[37,38] In this analysis, the free energy of an inhomogeneous, incompressible system with volume V is approximated by

$$G(\phi,\nabla\phi)=\int_V [g(\phi)+\kappa(\nabla\phi)^2]dV, \tag{7}$$

where $g(\phi)$ is the free energy density of the homogeneous system, κ is a phenomenological constant which is a measure of the free energy penalty associated with concentration fluctuations, and ϕ is the volume fraction of the fluctuating species. Using this equation, Cahn demonstrated that the onset of spinodal decomposition is announced by a scattering maximum at $q=q_m$:

$$q_m=\frac{1}{2}\left[\frac{-d^2g/d\phi^2}{\kappa}\right]^{1/2}. \tag{8}$$

Furthermore, by postulating a linear relationship between mass flux and chemical potential (an Onsager relationship), it was predicted that scattered intensity at the peak, I_m, would grow exponentially with time, while q_m would be independent of time:

$$I_m=I_{m0}\ \exp(t/\tau_m), \tag{9}$$

where τ_m is related to the Onsager coefficient, Λ:

$$\frac{1}{\tau_m}=\frac{1}{2}\,\Lambda(-d^2g/d\phi^2)q_m^2. \tag{10}$$

Applying this theory to a pseudobinary $A/B/AB$ mixture we get

$$-\frac{d^2g}{d\phi_A^2}=2\chi-\frac{4}{N(1-\phi_{AB})}=2(\chi-\chi_s), \tag{11}$$

where χ_s is the value of χ at the spinodal point in the ternary mixture $\{\chi_s=2/[N(1-\phi_{AB})]\}$. Equation (11) was derived from Eq. (1) under the condition that ϕ_{AB} is constant, and is restricted to symmetric mixtures in which $\phi_A=\phi_B=(1-\phi_{AB})/2$ and $N=N_Av_A/v\approx N_Bv_B/v$. These simplifications are appropriate for spinodal decomposition experiments described in this paper.

The phenomenological constant in equation (7) is obtained by expanding $S^{-1}(q)$ in the limit of small q and equating 2κ to the coefficient of the q^2 term.[6,46,55] We present the result for symmetric mixtures with the additional simplification that the statistical segment lengths of the A and B are identical ($l_A=l_B=l$). Using results derived by Broseta and Fredrickson[46] we get

$$\kappa=(l^2/9)h(\phi_{AB},N/N_{AB}), \tag{12}$$

where function h is given by

$$h(\phi,\alpha)=\frac{1}{4}\left[\frac{(1-\phi)^2}{4}+\frac{\phi(1-\phi)}{4\alpha}\right]^{-2}\left\{\frac{(1-\phi)^2}{4}\left[1-\phi+\frac{2\phi}{\alpha}-\frac{\phi}{\alpha^2}\right]+\frac{\phi(1-\phi)^2}{8\alpha^2}+\frac{\phi^2(1-\phi)}{4\alpha^2}-\frac{\phi^2(1-\phi)}{4\alpha^3}-\frac{\phi^3}{8\alpha^4}\right\}. \tag{13}$$

Note that in the limit of $\phi_{AB} \to 0$ we obtain $h=1$ (regardless of N/N_{AB}) and κ reduces to de Gennes result for a 50/50 homopolymer blend.[3] Substituting Eqs. (11) and (12) into Eq. (8) we get

$$q_{m-\mathrm{Cahn}} = \left[\frac{9(\chi-\chi_s)}{2l^2 h(\phi,\alpha)}\right]^{1/2}, \tag{14}$$

where l, the average statistical segment length, is given by[6]

$$l^2 = \frac{l_A^2 + l_B^2}{2}. \tag{15}$$

Equations (13)–(15) can thus be used to predict the location of the scattering maximum during the early stages of spinodal decomposition without resorting to any adjustable parameters.

EXPERIMENTAL RESULTS ON EARLY STAGES OF SPINODAL DECOMPOSITION

The early stages of spinodal decomposition in A0, A10, and A20 blends were obtained by time resolved SANS. We define $t=0$ as the time at which the sample was removed from the annealing oven which was set to a temperature well in the single phase region. The sample temperature was measured directly by inserting a thermocouple and it was found that the sample temperature reached 25 °C in 5 min. The measured scattering profiles obtained from the A0 blend at selected values of t are shown in Fig. 7(a). At $t=7$ min a peak appears at $q_m = 31\ \mu\mathrm{m}^{-1}$. The scattering peak stays within the experimentally observable window for about 30 min before disappearing behind the beam stop. The data obtained from the A10 and A20 blends are similar and are shown in Figs. 7(b) and 7(c).

The time dependence of q_m for the three samples is shown in Fig. 8. The early stage of spinodal decomposition, characterized by a time-independent q_m, is clearly evident in the data obtained from the A0, A10, and A20 blends. The location of the scattering maximum, q_m, for the A0 blend stays nearly constant from $t=7$ min until about 20 min. The A10 blend exhibits qualitatively similar behavior and q_m is nearly independent until $t=30$ min. In contrast, the 20% blend shows unusual characteristics at very early times. From $t=10$ to 20 min we find that q_m increases with time implying a decrease in the characteristic phase size with time before reaching a time-independent value. Han and coworkers have also observed this effect and have attributed this observation to the fact that during the quenching process the blends spend finite amounts of time at several locations within the spinodal.[26,27] The smaller values of q_m observed in the very early stages are probably due to spinodal decomposition at temperatures greater than 25 °C. Although this effect is most noticeable in the A20 blend, the A0 and A10 blends also show a slight increase in q_m at very early times, presumably due to the same effect.

In all three samples we observed a time interval over which q_m was, within experimental error, independent of time. This is the classic signature of the "early" stage of spinodal decomposition.[37,38] In Fig. 9 we compare the theoretical prediction based on Eq. (14) (curve labeled Cahn)

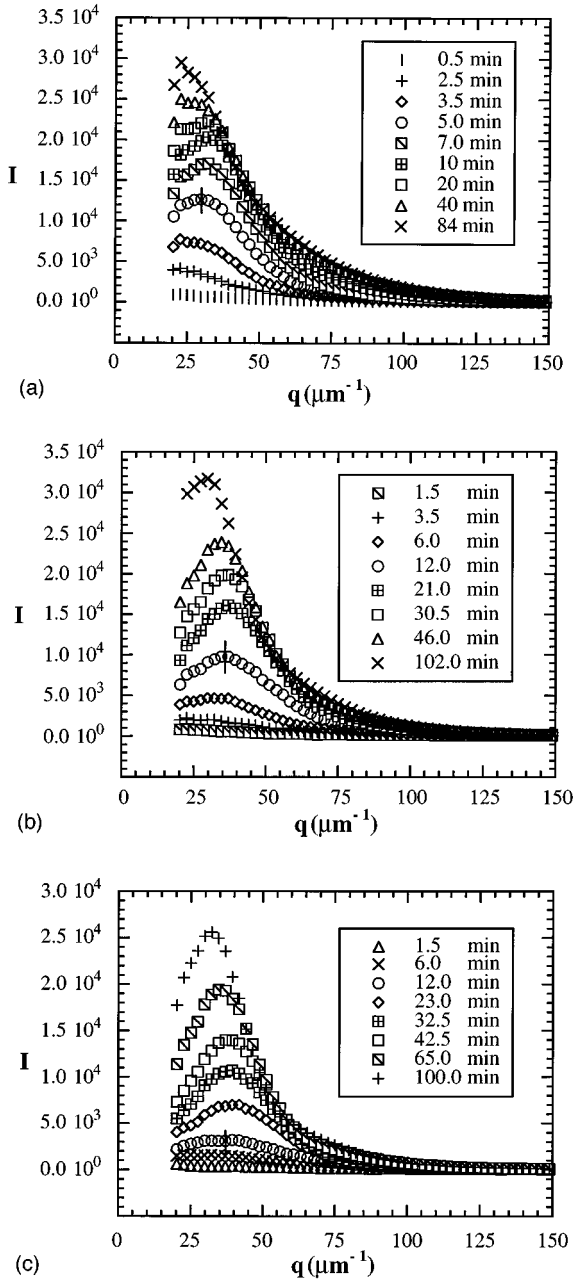

FIG. 7. Time-resolved SANS profiles at 25 °C. (a) A0. (b) A10. (c) A20.

with experimental results (squares). It is evident that the experimentally observed q_{m0} values are quite different from theoretical predictions. The largest deviation is observed in the binary blend (A0), where we find that theory overpredicts q_{m0} by a factor of 3. This is the blend with the largest value of χ/χ_s (see Table III). Blends A10 and A20, which have lower values of χ/χ_s, show better agreement with theory. This is consistent with de Gennes' assessment[4] that for deep quenches, the multiplicity of relaxation processes in polymer fluids[56,57] would make the Onsager coefficient q dependent. In such cases, Cahn's theory, which was developed for fluids with a q-independent Onsager coefficient (i.e., Newtonian fluids), would be inappropriate. A systematic description of this effect is contained in the work of Pincus and Binder.[5,6]

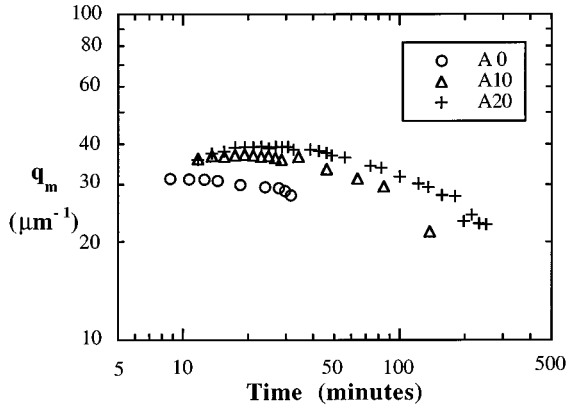

FIG. 8. The location of the time-resolved SANS maximum, q_m, vs time for blends A0, A10, and A20.

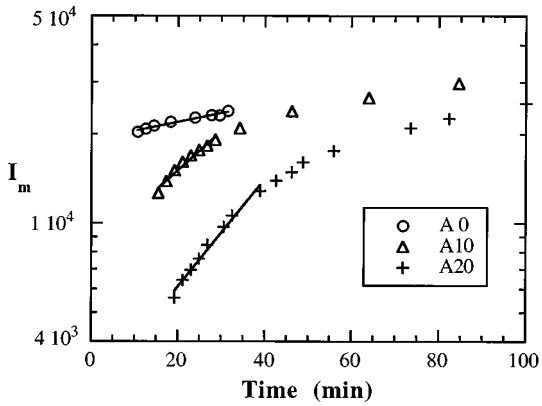

FIG. 10. The time dependence of the intensity at the time-resolved SANS maximum, I_m for blends A0, A10, and A20. The early stage, characterized by an exponential growth in I_m, is clearly evident.

The results of both theories can be summarized by the following equation:

$$\frac{q_{m-\text{deep quench}}}{q_{m-\text{Cahn}}} = s(\chi/\chi_s), \tag{16}$$

where function $s(\chi/\chi_s)$ is a monotonically decreasing function of quench depth χ/χ_s. For shallow quenches ($\chi/\chi_s \approx 1$), $s \to 1$. The functions obtained by Binder and Pincus are slightly different, due to slightly different forms used for the q dependence of Λ, and are given in Appendix B [Eqs. (B1) and (B2)]. However, for the χ/χ_s values of interest—1.0 to 2.5—the two theories give nearly identical values of $s(\chi/\chi_s)$.

Equations (16), (B1), and (B2) were derived for binary polymer blends and are thus only valid for A0 blend. Similar analyses for multicomponent mixtures have not yet been worked out. Lacking a better alternative, we computed the Pincus–Binder correction to the data from A10 and A20 blends, assuming that the same function $s(\chi/\chi_s)$ is applicable. The theoretical predictions based on the Pincus–Binder theory are in better agreement with experiments, as shown in Fig. 9. The discrepancy between theory and experiment is now less than a factor of 2. Note that the agreement in best at $\phi_{AB}=0.2$, suggesting that the pseudobinary approximation is not the main cause for the observed discrepancy. One possibility is that higher order corrections to the inhomogeneous free energy [Eq. (7)] may become important for describing deep quenches. On the other hand, the source of the discrepancy may lie in the experiments due to difficulties in performing rapid and deep quenches.

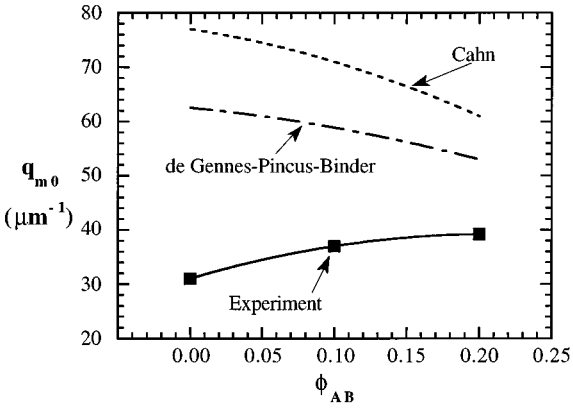

FIG. 9. The dependence of the early stage scattering peak, q_{m0}, on block copolymer concentration. The curves represent theoretical predictions based on Cahn theory (dotted curve), and on the de Gennes–Pincus–Binder theory (dot–dash curve).

The time dependence of I_m during the early stages (i.e., q_m independent of time) is shown in Fig. 10. Data obtained before q_m reaches a time-independent value are not shown. It is evident that I_m grows exponentially with time during the early stages, and that the addition of block copolymer leads to more rapid growth of the concentration fluctuations. Equation (10) could be used to estimate τ_m which, in turn, can be used to estimate Λ. According to de Gennes, for 50/50 homopolymer blends, $\Lambda = D_{\text{self}}N/4$, where D_{self} is the self-diffusion coefficient of the homopolymer. Self-diffusion coefficients can be estimated from rheological data. We estimate $D_{\text{self,PM}} = 4.5\times10^{-14}$ cm^2/s and $D_{\text{self,PE}} = 8.6\times10^{-13}$ cm^2/s. [$D_{\text{self}} = R_g^2/6\tau_d$ where the longest relaxation time, $\tau_d = 12\,\eta_0/(\pi^2 G_{n0})$, η_0 is the zero shear viscosity of the melt at room temperature (10^8 and 10^6 poise for PM and PE, respectively), G_{n0} is the plateau modulus (1.14 and 0.292 MPa for PM and PE, respectively).][58,59] Since the slower moving species is expected to dominate the relaxation processes,[6] we estimate that $\Lambda = 2.8\times10^{-11}$ cm^2/s. This is a factor of 20 larger than the experimental value obtained from A0, which is 1.4×10^{-12} cm^2/s. This factor is well outside experimental uncertainty, as well as corrections due to the q dependence of Λ.[5,6] The values of Λ discussed in this paragraph and in Table IV refer to the $q \to 0$ limit.

TABLE IV. Characteristics of the initial stages of spinodal decomposition.

Blend	Block copolymer vol. fr.	q_{m0} (μm^{-1})	I_{m0} (arb. units)	τ_m (min)	Λ (cm^2/s) $\times10^{12}$
A0	0.0	31	1.9×10^4	143	1.4
A10	0.1	37	8.2×10^3	33	5.1
A20	0.2	39	2.6×10^3	23	7.5

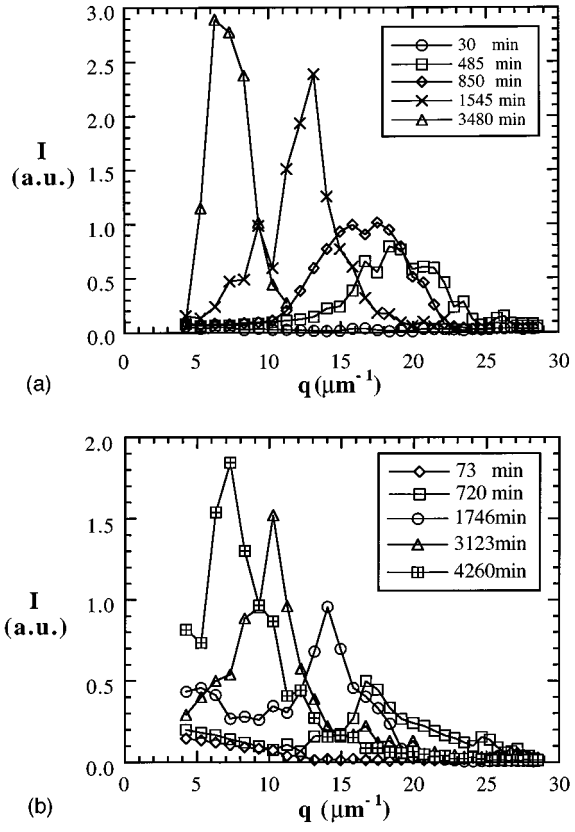

FIG. 11. The WALS profiles obtained from (a) A0 and (b) A20.

The long time data in Fig. 10 show gradual deviations from exponential growth, indicating the onset of the intermediate stage of spinodal decomposition. The points of departure from exponential growth are roughly consistent with the time at which q_m begins to decrease with time (Fig. 8). Most of the decomposition in this stage was beyond the q range of the SANS instrument and was studied by light scattering.

INTERMEDIATE AND LATE STAGES OF SPINODAL DECOMPOSITION

The coarsening of phase separated structure occurs in two stages: (1) the intermediate stage wherein both the composition and characteristic length of the coexisting phases change with time; and (2) the late stage wherein the composition of the coexisting phases and the intervening interface reach equilibrium and only the characteristic length increases with time.

Typical WALS profiles obtained from the A0 blend is shown in Fig. 11(a). The scattering profile is flat at early times ($t<500$ min). Note that the SANS results discussed in the preceding section indicate that the scattered intensity in the q range 10 $\mu m^{-1}<q<70$ μm^{-1} grows during the early stages. This is within the observable q window of the WALS apparatus. We believe that the lower optical contrast between the homopolymers precludes the possibility of observing the early stages on our light scattering instrument. However, with increasing time, the scattering intensity increases gradually and $t\approx500$ min a peaked scattering profile is clearly observed. As is typical of systems in the intermediate stage

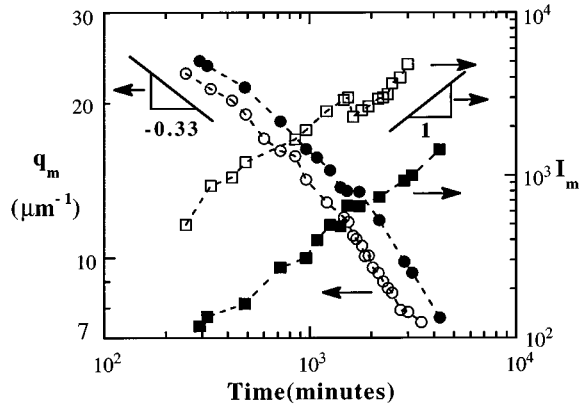

FIG. 12. The dependence of I_m and q_m on time plotted in log–log format. The solid lines represent scaling predictions of Akcasu *et al.* (Ref. 60) for the intermediate stage of spinodal decomposition. Solid symbols refer to blend A0 and open symbols refer to blend A20.

of spinodal decomposition, the peak moves to lower q and increases in intensity as time progresses. The time dependence of the scattering curves obtained from the A20 blend are similar and shown in Fig. 11(b).

In Fig. 12 we show the effect of block copolymer concentration on the time dependence of q_m and I_m. At any given time, t, we find that the blend containing the block copolymer has a smaller phase size (see q_m vs t data). This is a continuation of the trend observed during the early stages.

Coarsening processes in the intermediate stage are inherently nonlinear and analytical solutions to the governing equations are not possible. Approximate solutions were obtained by several researchers.[60–65] The results of these studies are often expressed as power laws

$$q_m=t^{-\alpha} \quad \text{and} \quad I_m\sim t^{\beta}. \tag{17}$$

Typical values for α in the intermediate stage range between 0.2 and 0.4. For instance, Akcasu and Klein predict that for polymer blends, α is 0.33 and β is 1 in the intermediate regime.[60] Due to dimensionality arguments β is equal to 3α. The theoretical work done thus far in the intermediate regime is restricted to binary blends.[60–65] The WALS data obtained from A0 and A20 are reasonably consistent with $\alpha=0.33$ and $\beta=1.0$. This suggests that the result of Akcasu and Klein, derived originally for binary polymer blends, is also valid for some multicomponent blends.

In theory, coarsening in the late stage is characterized by α and β values of 1 and 3, respectively.[63–65] Furthermore, since the structures obtained at different times are self-similar, differing only in length scale, a collapse of the scattering data are anticipated if Iq_m^3 is plotted vs q/q_m.[64,65] Typical SALS profiles obtained from the A0 and A20 samples are shown in Figs. 13(a) and 13(b), respectively. The qualitative features of the scattering profiles are a continuation of the trends observed in the WALS experiments: I_m increases with time while q_m decreases with time. In Figs. 14(a) and 14(b) we plot these data in Iq_m^3 vs q/q_m format. It is evident that the SALS data from A0 and A20 do not collapse over most of the available time window, implying that the blends are not in the late stage of spinodal decomposition. However, the last two sets of data obtained from A20 do

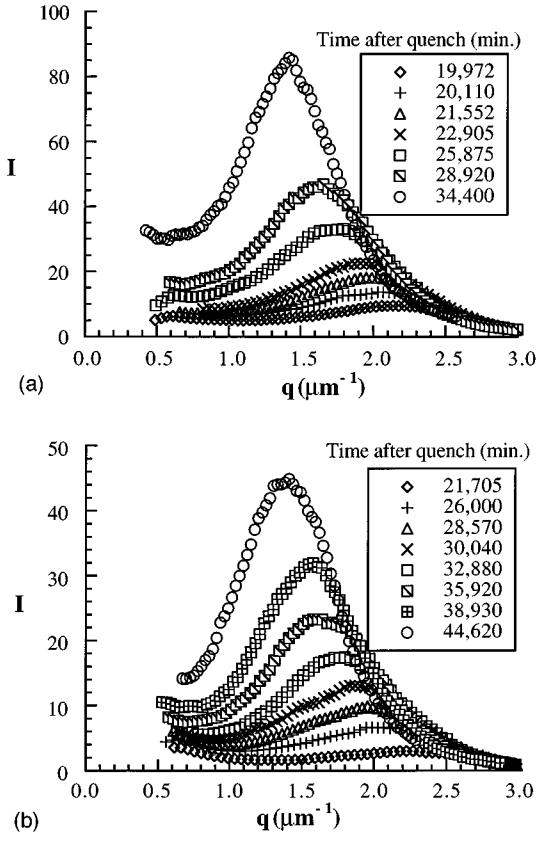

FIG. 13. The SALS profiles obtained from (a) A0 and (b) A20.

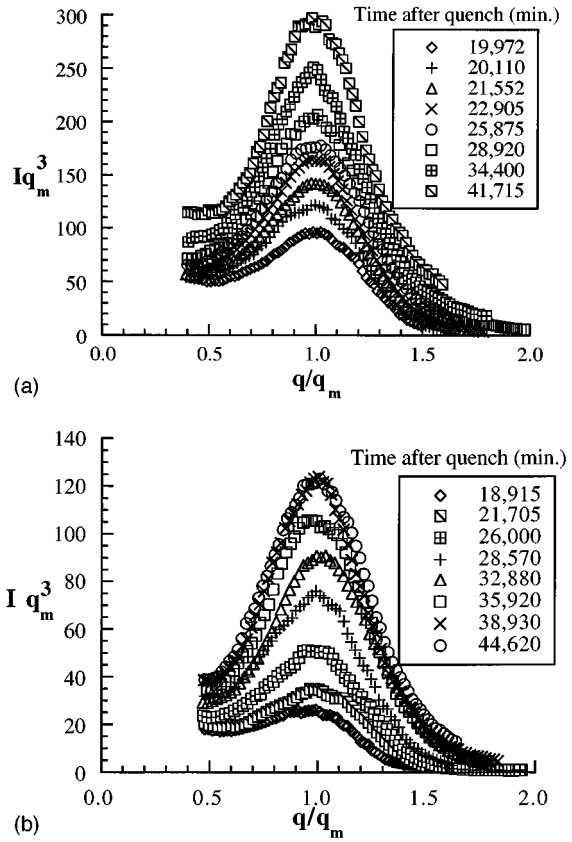

FIG. 14. The SALS data from (a) A0 and (b) A20 plotted in the format Iq_m^3 vs q/q_m. A collapse indicates the onset of the late stage of spinodal decomposition, and is only observed in the A20 blend after 4×10^4 min.

show some signs of collapse suggesting that the blend containing 20% block copolymer enters the late stage of spinodal decomposition after about 1 month! On the other hand, the A0 blend is still in the intermediate stage of spinodal decomposition after 1 month. This conclusion is consistent with data shown in Figs. 15 where we show the time dependence of q_m and I_m for the A0 and A20 blends. In the time window available, the values for α and β do not approach the expected values of 1 and 3, respectively.

We thus see that the addition of the PM-PE diblock to a PM-*B*/PE-*B* blend results in a more rapid approach toward the final stage of spinodal decomposition. These are the first experiments which demonstrate the possibility of acceleration of spinodal decomposition by addition of block copolymer. There are two possible reasons for this. First, the equilibrium concentrations are further apart in the 0% blend than in the 20% blend and thus achieving these concentration will require greater time (see Fig. 3). Second, the addition of the lower molecular weight diblock copolymer leads to a reduction in average viscosity which, in turn, can accelerate phase separation.

EFFECT OF BLOCK COPOLYMER ON SPINODAL DECOMPOSITION

We established experimentally that the block copolymer is homogeneously distributed in the one-phase region. However, as spinodal decomposition proceeds, and the concentration of the coexisting phases begin to diverge, the possibility of preferential segregation of the block copolymer at the interface increases. This may result in retardation of the spinodal decomposition due to ''crowding'' of the block copolymer molecules at the interface.[26,27] We do not see any evidence of this effect. The dependence of I_m and q_m on t obtained from the blend containing the block copolymer, A20, nearly parallels that found in the binary blend, A0. This is evident in the WALS data (Fig. 12) as well as the SALS data (Fig. 15). This indicates that the coarsening mechanisms

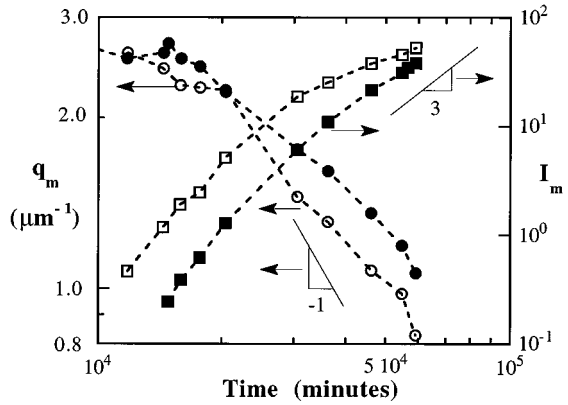

FIG. 15. The dependence of I_m and q_m on time plotted in log–log format. The solid lines represent scaling predictions for the late stage of spinodal decomposition (Ref. 60). Solid symbols refer to blend A0 and open symbols refer to blend A20.

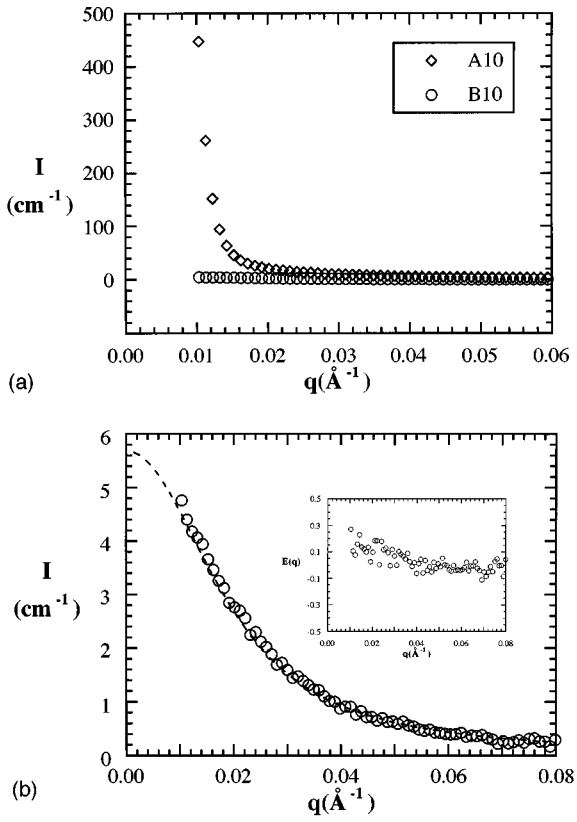

FIG. 16. (a) Absolute SANS intensity from blends A10 and B10 approximately 1.5 months after quenching from the single-phase to the two-phase region. In blend A10, the homopolymer PM-*B* is deuterated and the large forward scattering is typical of phase separated samples. In blend B10, the block copolymer PM-PE is deuterated and the scattering intensity is considerably reduced suggesting a lack of heterogeneity in the distribution of PM-PE. (b) The SANS intensity from B10 is compared to I_{ideal} for B10, and the near-quantitative agreement between I_{ideal} and SANS measurements confirms the lack of heterogeneity in the distribution of PM-PE. Inset: excess scattering function, $E(q)$, (cm^{-1}), for B10.

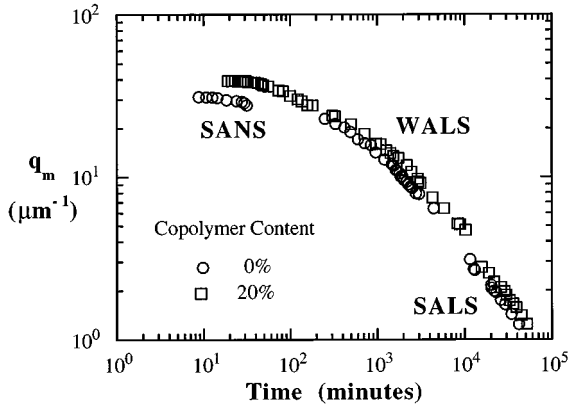

FIG. 17. A plot of q_m vs time, summarizing the evolution of structure in blends A0 (circles) and A20 (squares) over five decades of real time.

in the multicomponent blend (A20) are similar to those in the binary blend (A0). The phase size obtained from the block copolymer containing blend (A20) is smaller than that obtained from the binary blend (A0) at all times—Figs. 8, 12, and 15. Thus in a limited sense, one could argue that the addition of block copolymer slows down spinodal decomposition. However, more appropriate measures of the ''rate'' of spinodal decomposition are (1) value of the Onsager coefficient during the early stage, and (2) the time taken for the sample to enter the late stage of spinodal decomposition. On the basis of these criteria, we conclude that the addition of block copolymer leads to an *acceleration* of spinodal decomposition.

Direct evidence for uniform distribution of block copolymer in the late stages of spinodal decomposition is given in Figs. 16(a) and 16(b). In Fig. 16(a) we compare absolute SANS intensities from blends A10 and B10. These are PM-*B*/PE-*B*/PM-PE blends; the homopolymer PM-*B* is deuterated in A10, while the block copolymer PM-PE is deuterated in B10. These data were taken 15 weeks after quenching from the single phase region. The samples were turbid, and the light scattering signals from both samples were similar. A spinodal ring, indicating a phase size of about a micron, was evident. However, the SANS intensities from the two samples are in sharp contrast, as demonstrated in Fig. 16(a). The large scattering intensity in the forward direction in A10 is typical of phase separated samples. This suggests that the distribution of homopolymer PM-*B* (the labeled species) is nonuniform, especially at relatively large length scales (>500 Å). On the other hand, the small scattering intensity in the forward direction in B10 is atypical of phase separated

TABLE V. Parameters used for calculation of $I(q)$ of single-phase blends using RPA.

Parameter at 27°C	*h*PM-*A*	*d*PM-*A*	*h*PM-*B*	*d*PM-*B*	*h*PE-*A*	*d*PE-*A*	*h*PE-*B*	*d*PE-*B*	*d*PM-*d*PE (*h*PM-*h*PE)[a] PM block	*d*PM-*d*PE (*h*PM-*h*PE)[a] PE block
N_i	1105	1105	2465	2465	525	525	2630	2630	300(300)	300(300)
v_i (Å^3)	136.4	136.2	136.4	136.2	162.0	161.8	162.0	161.8	136.2(136.4)	161.8(162.0)
l_i (Å)	8.19	8.19	8.26	8.26	7.93	7.93	7.60	7.60	8.19(8.19)	7.93(7.93)
$b_i\times10^5$ (Å)	−4.15	5.33	−4.15	5.95	−4.98	6.14	−4.98	5.91	3.07(−4.15)	3.65(−4.98)

χ parameters between *d*PM and *h*PE are calculated according to Eq. (2).
χhPM/*d*PE$=1.85\times10^{-3}$ at 27°C (independent of molecular weight)
other χ parameters at 170°C
χhPM/*h*PE and χdPM/*d*PE$=6.0\times10^{-4}$ (independent of molecular weight)
χhPM-*A*/*d*PM-*A*$=7.8\times10^{-5}$ χhPM-*B*/*d*PM-*B*$=1.5\times10^{-4}$ χhPE-*A*/*d*PE-*A*$=9.6\times10^{-6}$ χhPE-*B*/*d*PE-*B*$=1.6\times10^{-6}$
all χ parameters based on a reference volume of 148.6 Å^3

[a]The characterization data of *h*PM-*h*PE are shown in the parentheses.

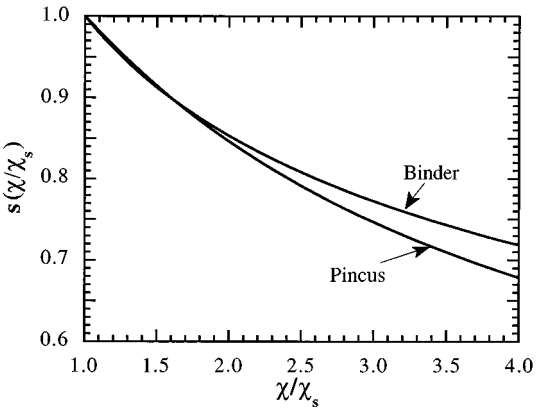

FIG. 18. A plot of $s(\chi/\chi_s)$ vs χ/χ_s.

samples. Since the block copolymer PM-PE is labeled in this blend, we conclude that qualitatively speaking, the nonuniformity in block copolymer distribution is minimal. In Fig. 16(b) we focus on the SANS signal from B10, which arises due to chain connectivity and concentration fluctuations of *d*PM-*d*PE. The dashed curve in Fig. 16(b) represents the connectivity contribution to the signal $[I_{\text{ideal}}(q)]$ and is calculated for blend B10 using Eq. (4) and parameters given in Appendix A, with all χ parameters set to zero. The absolute SANS intensity obtained from blend B10 is in very good agreement with this calculation. Consequently, the excess scattering function, $E(q)$, is nearly zero at all q [see inset in Fig. 16(b)]. Note that $E(q)$ for a phase separated sample is well defined; any mixture of polymers is single phase when all χ parameters are zero and thus $I_{\text{ideal}}(q)$ can be computed using RPA. Figure 16(b) provides *quantitative* evidence for the absence of block copolymer concentration fluctuations. Thus 15 weeks after quenching, we find that the block copolymer chains are uniformly distributed in the sample.

Based on very general arguments, Rice and Cahn have have shown that any third component that lowers the phase transition temperature of a binary mixture must, at equilibrium, be present in excess at the interface between coexisting phases.[66,67] Based on these works, one expects interfacial segregation of block copolymer in any phase separated mixture of two homopolymers and a block copolymer. Perhaps we were unable to detect this because the surface excess in PM-*B*/PE-*B*/PM-PE mixtures is not very large. On the other hand, it is possible that the surface excess may increase to detectable levels at a later stage (i.e., after 15 weeks).

CONCLUDING REMARKS

The spinodal decomposition of multicomponent, model polyolefin mixtures—polymethylbutylene, polyethylbutylene, and polymethylbutylene-*block*-polyethylbutylene—has been investigated following relatively deep quenches into the spinodal region (χ/χ_s range from 1.7 to 2.4). The evolution of the coexisting phases was studied by a combination of neutron and light scattering experiments. The dependence of the scattering maximum on time was monitored over 5 decades of real time. The results are summarized in Fig. 17. We find that the addition of block copolymer leads to a finer structure (larger q_m) over the entire time window. This may be used as a ''compatibilization'' effect. We, however, established that the block copolymer was uniformly distributed in the sample and not located preferentially at the interface. This is not what is usually observed in mixtures of two homopolymers and a block copolymer.[68] The early stages of spinodal decomposition, captured by time resolved SANS, were in qualitative agreement with the predictions of de Gennes, Pincus, and Binder. The coarsening characteristics in the blends with and without copolymer were found to be similar.

ACKNOWLEDGMENTS

We gratefully acknowledge the National Science Foundation for financial support. The work of C.C.L., H.S.J., and N.P.B. was supported by Grant No. CTS-9308164, Grant No. DMR-9307098, and the NSF Young Investigator Program, Grant No. DMR-9457950. The 30 m SANS instrument is supported by the NSF under Agreement No. DMR-9122444. We thank Ramanan Krishnamoorti and Bill Graessley for their many contributions toward the synthesis and characterization of the polymers used in this study, and John Cahn and Maurice Newstein for helpful discussions. We acknowledge John Barker, Charles Glinka, and Charles Han for their help during the SANS experiments.

APPENDIX A: PARAMETERS USED FOR MULTICOMPONENT RPA CALCULATIONS

In Table V we list the parameters at 27 °C used for multicomponent RPA calculation. Procedures used here are similar to those given in Ref. 28. We define the PM monomer to be a C_5H_{10} unit and the PE monomer to be a C_6H_{12} unit. The scattering lengths, b_i, and chain lengths, N_i, were estimated from characterization data. The monomer volumes, v_i, were calculated from densities and thermal expansion coefficients, α_i, of the homopolymers. The values of l_i were obtained form SANS experiments on 50/50 *h* PM/*d* PM and *h* PE/*d* PE mixtures.

The temperature dependence of v_i is assumed to be given by

$$v_i = v_{i,0} \exp(-\alpha_i(T-300)), \tag{A1}$$

where $v_{i,0}$ is v_i at 300 K. The temperature coefficients dl_i/dT are 7.0×10^{-4} (K^{-1}) and 6.5×10^{-4} (K^{-1}) for PM and PE segments, respectively.

APPENDIX B: THE EFFECT OF A NONLOCAL ONSAGER COEFFICIENT ON q_{m0}

Pincus and Binder arrive at the following equations for the location of the scattering maximum in the early stages of spinodal decomposition, q_{m0}, by accounting for the nonlocal (i.e., q dependent) nature of the Onsager coefficient:[5,6]

$$\frac{1-e^{-x}}{3} + e^{-x}(1-\chi/\chi_s + x/3) = 0 \quad \text{Pincus} \tag{B1}$$

and

$$\frac{x^2}{2\chi/\chi_s}+e^{-x}(x+1)-1=0 \quad \text{Binder,} \tag{B2}$$

where $x=q_{m0}^2Nl^2/6$ (see Appendix C for definitions of N and l). In the limit $\chi/\chi_s\to 1$, q_{m0} obtained from Eqs. (B1) and (B2) reduce to q_{m0} given by the Cahn theory [Eq. (14)]. The function $s(\chi/\chi_s)$ is defined as ratio of q_{m0} given by Eqs. (B1) and (B2) to $q_{m0\text{-Cahn}}$. In Fig. 18 we plot $s(\chi/\chi_s)$ vs χ/χ_s. It is evident from this figure that in the range of interest—χ/χ_s values between 1.7 and 2.4—the solutions to Eqs. (B1) and (B2) are nearly identical.

APPENDIX C: LIST OF SYMBOLS

b_i	scattering length of monomer i $(i=A,B)$
E	excess scattering from a mixture $(I\text{-}I_{\text{ideal}})$
f	volume fraction of block A in the block copolymer
g	Gibbs free energy per unit volume of a mixture
G	total Gibbs free energy of a mixture
I	scattered intensity
I_{ideal}	calculated coherent scattered intensity from a mixture due to chain connectivity only
I_m	coherent SANS intensity at the peak
l_i	statistical segment length of component i, obtained by fitting SANS data to mean-field theory
N	number of repeat units per homopolymer chain based on reference volume, v; $N=N_iv_i/v$
N_i	number of monomers per homopolymer chain $(i=A,\ B)$
$N_{i,b}$	number of monomers per block $(i=A,\ B)$
P	magnitude of the Kratky plateau (Iq^2 at high q) (μm^3)
q	scattering vector (μm^{-1})
q_m	scattering vector at the peak (μm^{-1})
q_{m0}	scattering vector at the peak during the early stages of spinodal decomposition (μm^{-1})
s	the ratio of q_{m0} derived from the theories based on nonlocal Onsager coefficients [Eqs. (B1) and (B2)] to that obtained from Cahn's theory [Eq. (14)]. This is only a function of χ/χ_s
t	time elapsed after a sample is quenched from single phase to room temperature
T	absolute temperature (K)
v	reference volume (equal to 148.6 Å^3 throughout this paper)
v_i	volume of a monomer $(i=A,B)$
χ_{ij}	Flory–Huggins interaction parameter, based on v
ϕ_i	volume fraction of component i $(i=A,B,AB)$

[1] *Polymer Blends*, edited by D. R. Paul and S. Newman (Academic, San Diego, 1978), Vols. 1 and 2.
[2] O. Olabisi, L. M. Roebling, and M. T. Shaw, *Polymer–Polymer Miscibility* (Academic, New York, 1979).
[3] P. G. de Gennes, *Scaling Concepts in Polymer Physics* (Cornell University, Ithaca, 1979).
[4] P. G. de Gennes, J. Chem. Phys. **72**, 4756 (1980).
[5] P. Pincus, J. Chem. Phys. **75**, 1996 (1981).
[6] K. Binder, J. Chem. Phys. **79**, 6387 (1983).
[7] T. K. Kwei, T. Nishi, and R. F. Roberts, Macromolecules **7**, 667 (1974).
[8] C. Herkt-Maetzky and J. Schelten, Phys. Rev. Lett. **51**, 896 (1983).
[9] G. Hadziioannou and R. S. Stein, Macromolecules **17**, 567 (1984).
[10] M. Shibayama, H. Yang, R. S. Stein, and C. C. Han, Macromolecules **18**, 2179 (1985).
[11] C. C. Han, B. J. Bauer, J. C. Clark, Y. Muroga, Y. Matsushita, M. Okada, Q. Tran-cong, T. Chang, and I. Sanchez, Polymer **29**, 2002 (1988).
[12] M. Warner, J. S. Higgins, and A. J. Carter, Macromolecules **16**, 1931 (1983).
[13] C. T. Murray, J. W. Gilmore, and R. S. Stein, Macromolecules **18**, 996 (1985).
[14] A. Maconnachie, R. P. Kambour, D. M. White, S. Rostani, and D. J. Walsh Macromolecules **17**, 2645 (1984).
[15] F. S. Bates, G. D. Wignall, and W. C. Koehler Phys. Rev. Lett. **55**, 2425 (1985).
[16] S. Sakurai, H. Hasegawa, T. Hashimoto, I. G. Hargis, S. L. Agarwal, and C. C. Han, Macromolecules **23**, 451 (1990).
[17] J. C. Nicholson, T. M. Finerman, and B. Crist, Polymer **31**, 2287 (1990).
[18] R. Krishnamoorti, W. W. Graessley, N. P. Balsara, and D. J. Lohse, Macromolecules **27**, 3073 (1994).
[19] N. P. Balsara, in *Handbook of Polymer Properties*, edited by J. E. Mark (AIP, New York, in press).
[20] T. Nishi, T. T. Wang, and T. K. Kwei, Macromolecules **8**, 227 (1975).
[21] T. Hashimoto, M. Itakura, and H. Hasegawa, J. Chem. Phys. **85**, 6118 (1985).
[22] M. Okada and C. C. Han, J. Chem. Phys. **85**, 5317 (1986).
[23] F. S. Bates and P. Wiltzius, J. Chem. Phys. **91**, 3258 (1989).
[24] D. Schwahn, S. Janssen, and T. Springer, J. Chem. Phys. **97**, 8775 (1992).
[25] M. Motowoka, H. Jinnai, T. Hashimoto, Y. Qiu, and C. C. Han, J. Chem. Phys. **99**, 2095 (1993).
[26] H. Jinnai, H. Hasegawa, T. Hashimoto, and C. C. Han, J. Chem. Phys. **99**, 4845 (1993).
[27] H. Jinnai, H. Hasegawa, T. Hashimoto, and C. C. Han, J. Chem. Phys. **99**, 8154 (1993).
[28] N. P. Balsara, S. V. Jonnalagadda, C. C. Lin, C. C. Han, and R. Krishnamootri, J. Chem. Phys. **99**, 10011 (1993).
[29] P. G. de Gennes, Faraday Discuss. R. Soc. Chem. **68**, 96 (1979).
[30] A. Z. Akcasu and M. Tombakoglu, Macromolecules **23**, 607 (1990).
[31] H. Benoit, M. Benmouna, and W. L. Wu, Macromolecules **23**, 1511 (1990).
[32] B. Hammouda, Adv. Polym. Sci. **106**, 87 (1993).
[33] J. W. Cahn, J. Chem. Phys. **42**, 93 (1965).
[34] J. W. Cahn, Trans. Am. Inst. Min. Eng. **242**, 166 (1968).
[35] J. E. Morral, J. W. Cahn, Acta Metall. **19**, 1037 (1971).
[36] R. J. Roe and C. M. Kuo, Macromolecules **23**, 4635 (1990).
[37] D. W. Park and R. J. Roe, Macromolecules **24**, 5324 (1991).
[38] T. Hashimoto and T. Izumitani, Macromolecules **26**, 3631 (1993).
[39] T. Izumitani and T. Hashimoto, Macromolecules **27**, 1744 (1994).
[40] H. Rachapudy, G. G. Smith, V. R. Raju, and W. W. Graessley, J. Polym. Sci., Polym. Phys. Ed. **17**, 1211 (1979).
[41] M. Morton and L. J. Fetters, Rubber. Chem. Tech. **48**, 359 (1975).
[42] Certain equipment and instruments or materials are identified in this paper in order to adequately specify the experimental details. Such identification does not imply recommendation by the National Institute of Standards and Technology, nor does it imply the materials are necessarily the best available for the purpose.
[43] A. R. Ramos and R. E. Cohen, Polym. Sci. Eng. **17**, 639 (1977).
[44] R. E. Cohen and A. R. Ramos, Macromolecules **12**, 131 (1979).
[45] L. Leibler, Makromol. Chem., Rapid Commun. **2**, 393 (1981).
[46] D. Broseta and G. H. Fredrickson, J. Chem. Phys. **93**, 2927 (1990).
[47] L. Leibler, Makromol. Chem., Macromol. Symp. **16**, 1 (1988).
[48] Z. G. Wang and S. Safran, J. Phys. (Paris) **51**, 185 (1990).
[49] M. L Huggins, J. Chem. Phys. **9**, 440 (1941).
[50] P. J. Flory, J. Chem. Phys. **9**, 660 (1941).
[51] R. L. Scott, J. Polym. Sci. **9**, 423 (1952).
[52] Equation (1) is not exact for mixtures studied in this paper because of the dependence of the χ parameter on deuterium substitution. However, this effect is relatively unimportant in the limited range of compositions examined in this paper (see discussion on p. 10091, Ref. 28).
[53] In previous studies by the Exxon/Princeton group on blends of ethylene–butene copolymers, (Ref. 54) it was found that near the spinodal, one had to wait for two weeks before the spinodal ring could be observed by light scattering. The molecular weights of the polyolefins used in these studies were less than 1.0×10^5 g/mol. The molecular weights of the polymers used in this study are a factor of 2 larger. Thus under equivalent conditions, one expects the waiting time to be an order of magnitude larger (on the basis that the characteristic time should scale with viscosity which in turn scales as $N^{3.4}$). Such long waiting times (about 1 month) per temperature, and the fact that such measurements have to be repeated at several

temperatures, makes it impossible to determine phase diagrams by light scattering. Nevertheless, we did try some light scattering experiments near the estimated critical points and found no increase in the forward scattering for several weeks.
[54] N. P. Balsara, L. J. Fetters, N. Hadjichristidis, D. J. Lohse, C. C. Han, W. W. Graessley, and R. Krishnamoorti, Macromolecules **25**, 6137 (1992).
[55] M. W. Matsen and M. Schick, Macromolecules **26**, 3878 (1993).
[56] P. G. de Gennes, J. Chem. Phys. **55**, 572 (1971).
[57] M. Doi and S. F. Edwards, *The Theory of Polymer Dynamics* (Oxford University, Oxford, 1986).
[58] J. T. Gotro and W. W. Graessley, Macromolecules **17**, 2767 (1984).
[59] W. W. Graessley and L. J. Fetters (unpublished data).
[60] A. Z. Akcasu and R. Klein, Macromolecules **26**, 1429 (1993).
[61] J. S. Langer, M. Bar-on, and H. D. Miller, Phys. Rev. **11**, 1417 (1975).
[62] M. Rao, M. H. Kalos, J. L. Lebowitz, and J. Marro, Phys. Rev. B **13**, 4328 (1976).
[63] E. D. Siggia, Phys. Rev. A **20**, 595 (1979).
[64] H. Furukawa, Physica A **123**, 497 (1984).
[65] K. Binder and D. Stauffer, Phys. Rev. Lett. **33**, 1006 (1974).
[66] O. K. Rice, J. Chem. Phys. **64**, 4362 (1976).
[67] J. W. Cahn, in *Interfacial Segregation*, edited by W. C. Johnson and J. M. Blakely (ASM, Metals Park, OH, 1979), p. 3.
[68] R. J. Roe and D. Rigby, Adv. Polym. Sci. **82**, 103 (1987).